Optimized Design of Filterless Horseshoe Networks Exploiting Point-to-Multipoint Coherent Transceivers

MOHAMMAD M. HOSSEINI[1,*], JOÃO PEDRO[2,3], ANTONIO NAPOLI[4], NELSON COSTA[2], JAROSLAW E. PRILEPSKY[1], AND SERGEI K. TURITSYN[1]

[1] *Aston Institute of Photonics, Aston University, Birmingham, UK*
[2] *Optical Architecture Group, Infinera Unipessoal Lda, Carnaxide, Portugal*
[3] *Instituto de Telecomunicações, Instituto Superior Técnico, Lisboa, Portugal*
[4] *Strategy, Architecture, and Engineering, Infinera, Munich, Germany*
[*] *Corresponding author: m.hosseini@aston.ac.uk*

Compiled September 16, 2023

The horseshoe topology is widely used to realize metro-aggregation networks, since it provides a natural fit to the hub-and-spoke traffic pattern present in the majority of these deployments, while enabling survivability against single link and hub failures. A filterless architecture can also be adopted to further reduce capital expenditure (CapEx) by replacing active elements, such as reconfigurable add/drop multiplexers (ROADMs), with simpler and passive splitters/combiners. Such an architecture can effectively host coherent-based point-to-multipoint (P2MP) transceivers enabled by digital subcarrier multiplexing (DSCM). Importantly, by carefully optimizing the deployment of amplifiers (location and gain) and splitters/combiners (type) it may be possible to reduce the total number of optical amplifiers required, further decreasing CapEx. This paper proposes an integer linear programming (ILP) framework to optimize metro-aggregation filterless horseshoe networks, taking into account the specific requirements of digital subcarrier multiplexing (DSCM)-based P2MP coherent transceivers. The results indicate a considerable reduction in amplifier count is possible while ensuring that end-to-end performance thresholds are met, which include the minimum required input power at the receivers, a maximum subcarrier input power difference at the hub's receivers, and the minimum optical-signal-to-noise ratio (OSNR).

http://dx.doi.org/10.1364/ao.XX.XXXXXX

1. INTRODUCTION

The advent of high-speed, low-latency, cost-effective, and reliable Internet infrastructure holds the key to unlocking the full potential of current and emerging technologies and applications such as the Internet of Things (IoT), cloud and 5G/6G services. Access and metro networks are crucial to provide services by aggregating and distributing IP traffic. They are usually non-meshed physical topologies predominantly supporting a hub-and-spoke traffic pattern, since the vast majority of traffic is exchanged with network segments outside of the region. For example, typical passive optical networks (PON) benefit from single-stage tree or multistage tree topologies, which are suitable for point-to-multipoint (P2MP) infrastructure deployment [1]. The widespread adoption of P2MP in access networks, in the form of PONs, has been able to reduce the cost per subscriber and minimize the amount of active equipment. The higher capacity and stringent survivability requirements of metro-aggregation networks demand a different transmission technology and topology. Common topologies include horseshoe [2], ring [3], and mesh [4], or a combination of them.

In network planning and topology design, sharing resources is a crucial concept for cost reduction. Cost-efficient solutions can be achieved by avoiding under-utilization or over-provisioning. One example of this is in dense wavelength division multiplexing (DWDM) systems. Multiple lightpaths connecting different node pairs can share a single optical fiber and utilize different frequencies to prevent interference, and produce a significant reduction in optical fiber costs. Similarly, the use of a single wavelength for serving multiple endpoints [5] in a time-division multiplexing (TDM)-PON reduces the amount of fiber and central office (CO) equipment needed compared to P2P architectures.

Compared to point-to-point (P2P) coherent pluggable transceivers, P2MP transceivers enabled by digital subcarrier multiplexing have shown potential to more cost-effectively support a hub-and-spoke traffic pattern in metro-aggregation networks [6]. In particular, this technology allows consolidating multiple low-capacity flows in a single high-capacity device at the hub nodes, improving key metrics such as cost, power consumption, and footprint. In contrast, typical P2P solutions rely on pairing transceivers at the hub and leaf nodes, which requires hosting multiple transceivers at the hub node. The feasibility of this technology has been experimentally verified in recent works [7].

Our previous research has focused on examining DSCM-based P2MP cost savings in ROADM-based [8], and filterless [9] meshed metro-aggregation networks. Here we will look more closely at the physical design of optical nodes. Splitters/combiners have been used at optical nodes in filterless optical networks to optically broadcast light downstream from hub node(s) to leaf nodes and groom digital subcarriers (DSCs) from leaf nodes to hub node(s) in the upstream direction. It is worth noting that optical signals go through different loss/amplification stages as they travel via different paths and traverse several splitters/combiners, fiber spans and optical amplifiers.

A horseshoe topology can provide single-point failure protection by allowing two disjoint paths from every leaf node to two hub nodes to be set up. Protection against link and hub failures increases network resiliency and, consequently, quality of service [10–12]. This paper extends our seminal work on the physical design of filterless horseshoe networks supporting P2MP transceivers [13]. First, it provides a more detailed description of an integer linear programming framework tailored for jointly optimizing the splitters/combiners selection at leaf nodes and the amplifier placement in a filterless horseshoe network supporting DSCM-based P2MP transceivers. The main optimization objective is to minimize the number of optical amplifiers required while guaranteeing that different system-level constraints are met. In [14], the authors have presented two amplifier placement methods to optimize the number of amplifiers in metropolitan wavelength-division-multiplexing (WDM) rings based on non-linear and linear integer programming techniques. In addition, some heuristics have been developed in [15] to address the amplifier placement problem in metro networks. Moreover, horseshoe topologies can be planned as flexible semi-filterless networks for metro DWDM applications [16], where a fixed unbalanced splitter/combiner has been used to add and drop signals. A dual node architecture, combining filterless and filter-based elements for low-cost C+L-band communication, has been studied in [17].

Additionally, this work presents a more comprehensive analysis of the framework's performance by (i) considering multiple instances of the problem (e.g., different network sizes, randomly generated fiber span lengths), (ii) including the required optical signal-to-noise ratio in the feasibility assessment; and (iii) evaluating the scalability of the framework (e.g., execution time). The simulation results highlight the correlation between optical amplifier savings and the diversity of splitter/combiner types available for deployment.

The rest of the article is structured as follows. In Sec. 2, we describe the DSCM-based P2MP transceiver architecture and function. Sec. 3 details the network architecture being considered, as well as a mathematical model for generating physical topologies that exploits empirical data to statistically ensure network results. Sec. 4 describes the ILP-based optimization framework (input parameters, variables, and formulation) proposed for the optimized deployment of amplifiers and splitters/combiners, while meeting specific design constraints. A comprehensive set of results is presented and discussed in Sec. 5. Finally, Sec. 6 highlights the main conclusions of this work.

2. DIGITAL SUBCARRIER MULTIPLEXING P2MP COHERENT TRANSCEIVERS

Multi-carrier solutions that lower the symbol rate of individual subcarriers (SC) have been proposed to mitigate the impact of symbol rate on the nonlinearity of coherent transmission [18–20]. Orthogonal frequency-division multiplexing (OFDM) and Nyquist multiplexing are two methods for creating SCs. It is possible to generate them digitally at the transmitter within the digital signal processor (DSP) and load the samples to the digital-to-analog converters (DACs). Because the spectra of the individual DSCs created by the Nyquist multiplexing method do not overlap (not the case in the OFDM counterpart), the individual SCs can be isolated and processed independently [21]. In addition, SC multiplexing reduces the complexity of dispersion compensation compared to the single carrier approach [22]; however, it can slightly increase the optical-signal-to-noise-ratio (OSNR) penalty [23]. Overall, this technique has shown to be a key element in building high performance transceivers, such as the 800G commercial solutions being deployed in regional and long-haul networks [24].

Importantly, DSCM is also the fundamental building block for realizing coherent transceivers that enable P2MP connectivity in the optical domain [7]. With this architecture, a high-capacity transceiver, located at a hub node, slices the spectrum of an optical channel and allocates it to several SCs, which are then broadcast towards a set of leaf nodes. Each leaf node is equipped with a low data rate transceiver that can receive and process the correct subset of SC(s). These low data rate transceivers can transmit the sub-set of SCs upstream towards the high-capacity transceiver of the hub node. Note that the sub-sets of non-overlapping SCs that are generated at the different leaf nodes can be optically merged (e.g., using a passive combiner) in their path towards the hub node. One of the primary advantages of using P2MP transceivers is that fewer interfaces in switches/routers are needed at the hub, resulting in lower complexity and capital expenditure (CapEx). These higher capacity P2MP transceivers also offer a lower cost per transmitted bit and have been shown to assist in reducing over-provisioning and under-utilization of resources [9].

3. METRO-AGGREGATION NETWORK ARCHITECTURE

Tree and horseshoe topologies are the main candidates to realize metro-aggregation networks exploiting a filterless architecture, although more complex (i.e., meshed) topologies can also be utilized [8]. In a filterless architecture, optical filters, such as the ones using wavelength selective switches (WSSs) or arrayed waveguide gratings (AWGs), are replaced by simple splitters/combiners which broadcast/merge optical signals without the capability to differentiate optical frequencies: the entire optical spectrum is transmitted [17]. This limits the ability to perform selective power equalization and wavelength reuse. The latter is a key capability in regional and long-haul networks, since they tend to have more meshed traffic patterns and

need to support significantly higher traffic loads. Conversely, filterless network architectures have found application in access networks, where traffic requirements are very low compared to fiber capacity, the hub-and-spoke traffic pattern copes well with the inability to support wavelength reuse, and transmission distances are short. According to Ethernet PON standards, optical signals can tolerate a 20 km distance and a 1:32 split ratio. Different generations of PON networks, such as G-PON [25] and WDM-PON, have been proposed to provide more capacity and reach. An optimized design of the network topology can reduce the cost of PONs deployment. In [26], the cost of connecting every end point to the central offices (COs) was studied under realistic restrictions, such as possible fiber paths, the splitting ratio of optical splitters, and locations of COs when a set of possible locations are given. The use of adjusted splitting ratios of asymmetrical splitters, in order to fit area characteristics, has shown a gain of 6.1 dB in the power budget in specific areas [27]. Cost, bandwidth per user, split ratio, maximum reach, and ease of maintenance are crucial aspects of commercial success [28].

Metro-aggregation networks sit between access networks and metro-core/regional networks. They tend to feature a hub-and-spoke traffic pattern, transmission distances of dozens to a few hundred kilometers and total traffic requirements of up to a few hundred Gb/s. These characteristics support the use of a filterless architecture, since the benefits of simplicity and cost-effectiveness are likely to outweigh the spectral and power inefficiencies of this architecture [29]. Moreover, filterless networks are inherently gridless and so are well-suited for elastic optical networking and innovative technologies like dynamic spectrum allocation.

A. Horseshoe Architecture

In this paper, the deployment of DSCM-based P2MP transceivers in horseshoe topologies with a filterless architecture is considered. Fig. 1 illustrates a metro-aggregation network architecture based on a horseshoe topology. It consists of two hub nodes, five leaf nodes, and six links. Each link is made of an optical fiber pair, and several passive optical splitters and combiners perform the drop and add functions. Optical amplifiers are placed before or after leaf nodes to compensate for losses. Every leaf node communicates with both hub nodes bidirectionally using disjoint paths (enforced by the topology) and separate transceivers at the leaf nodes. High resilience is guaranteed, since services can survive single-link and single-transceiver failures and even certain combinations of multiple failures. However, this architecture requires doubling the number of transceivers deployed and increases losses at each leaf node, due to the need to drop the SCs from one hub and insert the SCs directed at the other hub. It is worth noting that the transceivers can be plugged directly into routers (e.g., in QSFP-DD form factor at the hub router).

Importantly, in the upstream direction (i.e., from leaf nodes to hub node), the power levels of signals received at hub nodes from upstream SCs can vary. The receiver at the hub may be able to accommodate a certain difference in the power levels of SCs arriving from different leaf nodes. Note that a similar challenge arises in passive optical network (PON) systems, where optical packets travel through different paths, leading to variations in signal levels at the optical line terminal (OLT). This problem has been addressed by the use of an automatic gain control (AGC) approach [30] or optimized semiconductor amplifiers [31]. Ideally, the network should be designed such that no additional equipment is needed to meet this constraint. For instance, deploying splitters/combiners with asymmetrical ratios and placing amplifiers with the appropriate level of gains can help equalize SCs' power in filterless horseshoe networks. In addition, in both downstream and upstream directions, the network design must also honor the minimum input power level at each receiver for correct operation. Finally, it should also be guaranteed that the network is operated in a linear or quasi-linear regime, which imposes restrictions on the maximum launch power at the input of every fiber link.

B. Link Length Statistical Model

In general, evaluating the effectiveness of network design strategies should be accomplished by considering a wide set of problem instances to improve the statistical significance of the findings. In this work, we use the statistical properties from a set of real horseshoe topologies described in [2] to generate a larger set of topologies. In particular, we fit a log-normal distribution [32] in which the probability density function (PDF) is defined by the parameters μ and σ as follows:

$$f(x) = \frac{1}{x\sigma\sqrt{2\pi}} exp\left\{-\frac{(lnx-\mu)^2}{2\sigma^2}\right\}, \qquad for \quad x > 0. \tag{1}$$

In contrast to the normal distribution, the log-normal distribution handles the case of positive skewness, which we have observed to be present in the sample topologies. Fig. 2 shows a log-normal distribution with parameters of $\mu = 2.45$ and $\sigma = 0.41$ fitted to the empirical data. The average link length is 13.2 km, while the standard deviation is 5.65 km. The results reported in Sec. 5 were obtained by using this distribution to generate multiple horseshoe topologies, which are then designed using the optimization framework of Sec. 4.

4. OPTIMIZATION FRAMEWORK

In this section, we propose an optimization framework that comprises an ILP model to address the design of filterless horseshoe networks supporting P2MP transceivers. The objective of the optimization framework is to realize line system savings in terms of optical amplifiers, while ensuring that the different constraints for correct operation of the transceivers are met. Note that the optimization for each transmission direction, i.e., from Hub1 to Hub2 and from Hub2 to Hub1 (see Fig. 1), can be carried out independently. For the sake of simplicity, in the following, the proposed ILP model considers signal transmission from Hub1 to Hub2. The main input parameters and decision variables of the ILP model are listed as follows:

Input Parameters

- $G(V, E)$: graph with leaf nodes $u, u_p, v \in V$ and links $l \in E$,
- $W(u)$: length of the link that connects leaf u to its left-hand side node,
- α: fiber attenuation coefficient,
- $G_e(g)$: EDFA gain, a vector containing all possible gain values including 0 that means no amplifier,
- P_{sc}: launch power per SC,
- P_n: threshold nonlinear power per SC,
- P_s: sensitivity power level,
- P_l: maximum power difference tolerance of SCs,
- $H(s, p)$: insertion loss of splitter/combiner s at port p.

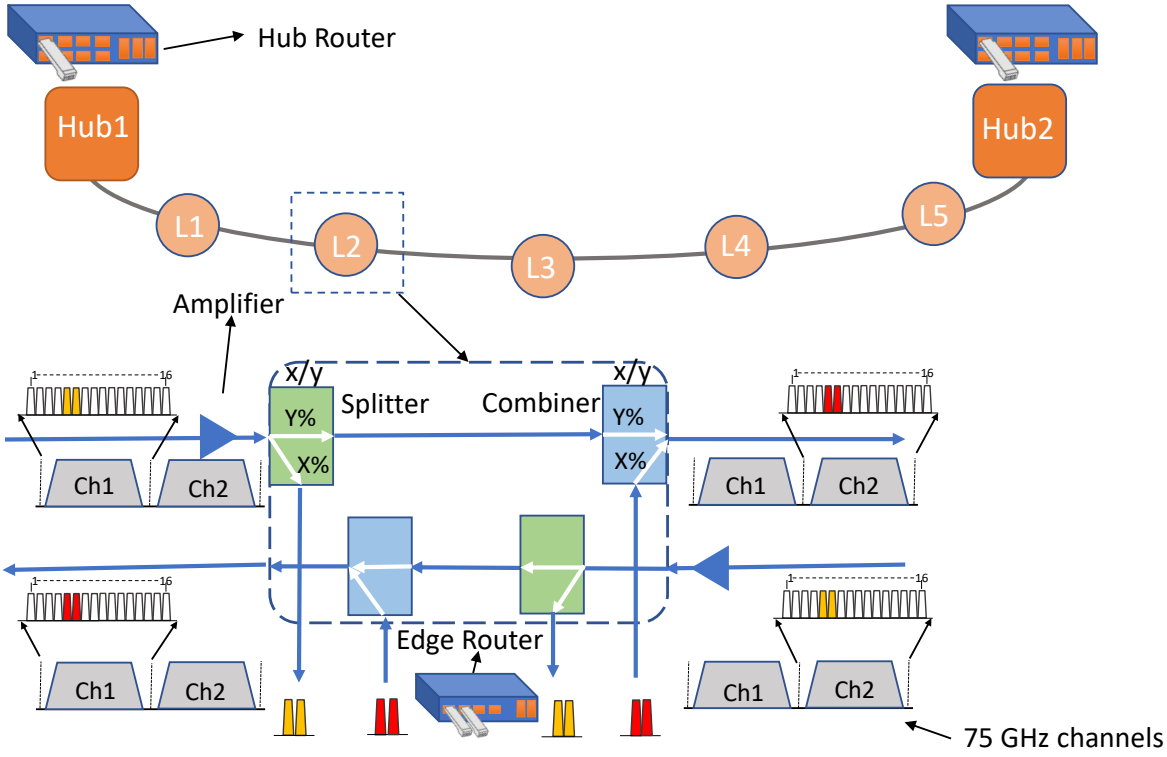

Fig. 1. Illustration of a filterless horseshoe network and DSCM-based P2MP transceiver deployment using passive optical splitters/combiners.

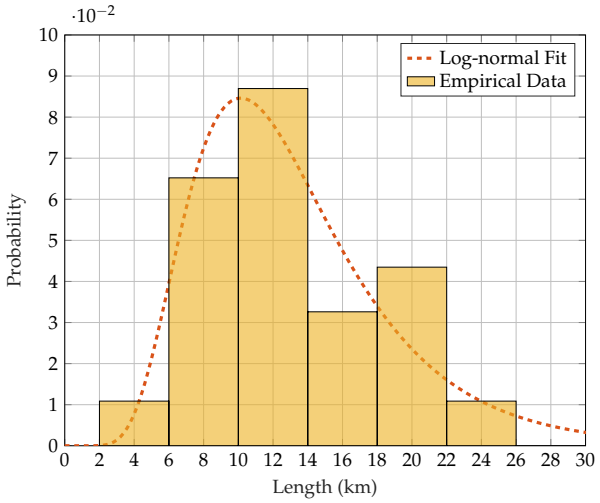

Fig. 2. Log-normal distribution fitted to the length of optical links data from real networks.

Decision Variables

- Δ_s^u: binary variable for combiner selection; 1 if combiner s is selected for leaf u, 0 otherwise,
- ∇_s^u: binary variable for splitter selection; 1 if splitter s is selected for leaf u, 0 otherwise,
- γ_p^u: loss of port p of combiner selected for leaf u,
- δ_p^u: loss of port p of splitter selected for leaf u,
- μ_g^u: binary variable; 1 if amplifier at leaf u takes gain g,
- ϕ_u^1: Hub2 receiver (Rx) power per SC coming from leaf u,
- ϕ_u^2: leaf u Rx power per SC coming from Hub1,
- ϵ_1: lower bound of variables ϕ_u^1,
- ϵ_2: upper bound of variables ϕ_u^1.

Eq. 2 expresses the objective function of the ILP model and comprises two terms. The first term corresponds to the primary objective of the ILP model, which is to minimize the number of optical amplifiers deployed in the network. A secondary goal is embedded in the objective function and consists of minimizing the difference between the highest and lowest power levels of the SCs reaching the receiver (Rx) of Hub2. The weight factor w must be large enough to ensure that the highest priority is to minimize the number of amplifiers. The model will thus not only meet the maximum power difference tolerance of SCs, which is described below in the constraints, but will also try to further reduce that difference, with the aim of operating the hub's receiver further from the limit and closer to optimal conditions.

$$z = \sum_u \sum_{G_e(g)\neq 0} \mu_u^g + w[\epsilon_2 - \epsilon_1], \tag{2}$$

subject to the constraints as follows:

$$\sum_s \Delta_s^u = 1 \quad \forall u \in V, \tag{3}$$

$$\sum_s \nabla_s^u = 1 \quad \forall u \in V, \tag{4}$$

$$\gamma_p^u = \sum_s \Delta_s^u H(s,p) \quad \forall u \in V, \tag{5}$$

$$\delta_p^u = \sum_s \nabla_s^u H(s,p) \quad \forall u \in V, \tag{6}$$

$$\sum_{g} \mu_g^u = 1 \quad \forall u \in V, \tag{7}$$

$$\phi_u^1 = P_{sc} + \sum_{v>u} \sum_{g} G_e(g)\mu_g^v - \alpha \sum_{v>u} W(v) - \gamma_{p_1}^u - \sum_{v>u} (\gamma_{p_2}^v + \delta_{p_2}^v) \quad \forall u \in V, \tag{8}$$

$$\phi_u^2 = P_{sc} + \sum_{v\le u} \sum_{g} G_e(g)\mu_g^v - \alpha \sum_{v\le u} W(v) - \delta_{p_1}^u - \sum_{v<u} (\gamma_{p_2}^v + \delta_{p_2}^v) \quad \forall u \in V, \tag{9}$$

$$P_{sc} + \sum_{v\le u} \sum_{g} G_e(g)\mu_g^v - \sum_{v\le u} (\gamma_{p_2}^v + \delta_{p_2}^v) - \alpha \sum_{v\le u} W(v) \le P_n \quad \forall u \in V, \tag{10}$$

$$P_{sc} + \sum_{u_p<v\le u} \sum_{g} G_e(g)\mu_g^v - \sum_{u_p<v\le u} (\gamma_{p_2}^v + \delta_{p_2}^v) - \alpha \sum_{u_p<v\le u} W(v) - \gamma_{p_1}^{u_p} \le P_n \quad \forall u, u_p \in V, \tag{11}$$

$$\epsilon_1 \le \phi_u^1 \quad \forall u \in V, \tag{12}$$

$$\epsilon_2 \ge \phi_u^1 \quad \forall u \in V, \tag{13}$$

$$\phi_u^1 \ge P_s \quad \forall u \in V, \tag{14}$$

$$\phi_u^2 \ge P_s \quad \forall u \in V, \tag{15}$$

$$\epsilon_2 - \epsilon_1 \le P_l. \tag{16}$$

Constraints (3) and (4) select an index of combiners and splitters while constraints (5) and (6) assign the corresponding loss of combiners and splitters to different ports. An optical amplifier with non-zero gain g is located right before leaf u through constraint (7) (gain 0 means no amplifier is required at that location). Constraints (8) and (9) calculate the per SC power received by Hub2 from leaf nodes and the per SC power received by leaf nodes from Hub1, respectively. Constraint (10) and constraint (11) ensure that the power per SC does not exceed the nonlinearity threshold power on optical fibers downstream (Hub1 to leaf nodes) and upstream (leaf nodes to Hub2), respectively. Note that this threshold is defined so as to be able to operate in a linear regime, i.e., assuming that the impact of nonlinear interference in optical performance is negligible. The lower bound and upper bound of the power levels received by Hub2 are determined by constraints (12) and (13). Constraints (14) and (15) guarantee that received powers meet the sensitivity requirement of the transceivers. Constraint (16) ensures that the difference between the highest and lowest SCs power does not exceed the threshold defined.

To implement a scenario where amplifiers are positioned immediately after leaf nodes, we have to modify only the amplifiers' gain terms in Eq (8,9,11) to consider the booster amplifiers configuration instead of the pre-amplifiers setup. Terms $\sum_{v\ge u}\sum_g G_e(g)\mu_g^v$, $\sum_{v<u}\sum_g G_e(g)\mu_g^v$, and $\sum_{u_p\le v\le u}\sum_g G_e(g)\mu_g^v$ have to be used in Eq. (8), Eq. (9), and Eq. (11), respectively.

over

At each leaf node, the ILP model is performing different decisions. These include the type of splitter and the type of combiner to deploy, out of a list of $|s|$ types, where each type is characterized by a particular splitting ratio. Note that not only the type of device is defined but also how it is deployed: for devices with an asymmetrical splitting ratio, which of the ports is used for adding (combiner) or dropping (splitter) and which is used for expressing the SCs. A key decision is the gain of each optical amplifier, assuming a discrete set of $|g|$ gain values that includes the option of setting the gain to zero, which corresponds to skipping the use of an amplifier at that specific location. For a horseshoe network with $|u|$ leaf nodes, the solution search space for each transmission direction has a size of $(|g| \times 2|s| \times 2|s|)^{|u|}$. The maximum computational complexity of an ILP problem can be established based on the number of decision variables and constraints in the problem instance. In the case of our optimization framework, the number of variables is $|u|(6+4|s|+|g|+2)$ and the number of constraints is $14|u| + |u|(|u|-1)/2 + 1$ for Scenario1. Note that the actual computational complexity and computation time can vary greatly depending on the specific problem instance, and the computational time of two instances of the same problem can differ significantly due to the various paths to optimal solutions.

The quality of signal recovery in optical communication systems depends on the optical signal-to-noise ratio (OSNR). The accumulation of amplified spontaneous emission (ASE) noise from optical amplifiers, such as Erbium-doped fiber amplifiers (EDFAs), along the transmission path can have a significant impact on the OSNR. Therefore, it is essential to accurately measure and quantify the ASE noise in EDFA's to ensure optimal signal recovery. The ASE noise in an EDFA can be presented as follows:

$$P_{ASE} = m n_{sp} h\nu (G-1) B_{ref} \tag{17}$$

where m represents the number of polarization modes (1 or 2), n_{sp} is the spontaneous emission factor, h is the Planck constant, G is amplifier gain, and B_{ref} is usually considered the bandwidth equivalent to the 0.1 nm band around 1550 nm. As a result, the OSNR at the output of an EDFA is approximated by [33]:

$$OSNR[dB] \approx P_{signal}^{in}[dBm] - NF[dB] + 58 \tag{18}$$

where P_{signal}^{in} is the power of the optical signal at the input of the amplifier, and NF is the amplifier's noise figure. The total OSNR, however, depends on the number of times a signal is amplified. It can be formulated in linear units, as Eq.19:

$$\frac{1}{OSNR_t} = \frac{1}{OSNR_1} + \frac{1}{OSNR_2} + ... + \frac{1}{OSNR_n} \tag{19}$$

in which $OSNR_t$ is the total OSNR, and $OSNR_n$ is n_{th} amplifier. It is worth noting that the total OSNR is smaller than the smallest individual OSNRs. Importantly, it is not possible to express with linear terms the OSNR at each receiver as a function of the different OSNR contributions along the transmission path. Therefore, to preserve the ability to use an ILP model that can be optimally solved, the OSNR at each transmission path is assessed and compared to the OSNR threshold in a post-processing stage after executing the ILP model.

5. RESULTS AND DISCUSSION

This section reports the results of applying the described optimization framework to the design of metro-aggregation horse-

shoe topologies. We assume that the transceivers communicate using dual-polarization 16-QAM modulation format at 4 GBd per subcarrier, which results in a 25 Gb/s payload per SC. The minimum input power at the receiver is $P_s = -24$ dBm per SC and the required OSNR is 12 dB per SC. These values were derived from the OpenZR+ multi-source agreement (MSA) [33] and have been scaled to consider 4 GBd SCs, instead of the original 60.1 GBd single carrier signal. Although the launch power can be variable within a given range, we consider $P_{sc} = -12$ dBm launch power per SC for both leaf nodes and hub node transceivers. Note that this corresponds to a maximum output power of 0 dBm when considering all 16 SCs that can be generated at the hub's transmitter to create a 400 Gb/s signal, which is aligned with commercial offerings for 400 Gb/s pluggable transceivers. The noise figure of each amplifier is assumed to be 5 dB when operating in the range of gain values considered. As described above, the design assumes that nonlinear interference due to transmission in the optical fiber must be reduced to the point that it has a negligible impact on optical performance. Hence, the power per SC must not exceed the nonlinearity power threshold at any point along the optical fibers. Given that only EDFAs are used, the highest power level is observed at the start of the fiber links. The non-linearity power threshold considered is $P_n = -10$ dBm per SC, and this restriction is modelled via constraints (10) and (11) of the ILP model of section 4.

In the proposed filterless horseshoe architecture, 1:2 splitters/combiners can be employed at the leaf nodes as we assume only one transceiver per transmission direction is expected to be required. Table 1 shows a list of balanced and unbalanced splitters/combiners ratios and their equivalent port losses in dB. In addition to split/combine loss, other types of loss occur inside splitters/combiners. Excess loss is the difference between the sum of powers entering the output ports in each fundamental mode and the power exiting the device in the fundamental input mode [34]. In this investigation, a constant 0.5 dB additional loss is assumed to account for losses other than power division loss. It is important to note that the splitters/combiners under examination are four-port optical coupler devices that utilize fusion technology. To prevent reflections, one of the ports is matched within the device [35].

Table 1. List of 1:2 splitters/combiners as well as ports insertion losses in dB in ideal and realistic cases.

Splitting Ratio [%]		Ideal Insertion Loss [dB]		Realistic Insertion Loss [dB]	
port 1	port 2	port 1	port 2	port 1	port 2
50	50	3.01	3.01	3.51	3.51
60	40	2.22	3.98	2.72	4.48
70	30	1.55	5.23	2.05	5.73
80	20	0.97	6.99	1.47	7.49
90	10	0.46	10	0.96	10.5

Horseshoe networks comprising 5, 10, and 15 leaf nodes are considered. The length of the optical fibers is randomly generated according to the log-normal distribution described by Eq. 1. In the following, all results shown are obtained using 100 independent simulation runs. The fiber attenuation coefficient is $\alpha = 0.22$ dB/km for every fiber link. We assume the optical amplifiers can provide a gain value between 6 dB and 20 dB with 1 dB granularity. The maximum power difference of SCs that can be tolerated at Hub receiver P_l is set to 8 dB.

It should be noted that while amplifiers can theoretically be positioned at any point along the optical links, their performance can vary with location. According to the simulation results presented in Table. 2, if the amplifiers are placed only immediately after the leaf nodes, the number of amplifiers required for Scenario1 and Scenario2 would be 5.5 and 7 respectively. These numbers are significantly higher than when the amplifiers are placed before the leaf nodes. For the other two scenarios, this configuration is not able to provide a feasible solution for most of the network instances. Placing amplifiers immediately after the leaf nodes poses limitations on the achievable gain due to nonlinearity constraints. Placement before the splitter and combiner, instead of after these devices, has a two-fold advantage: (i) the SCs that will be locally processed are amplified just before being dropped, facilitating meeting the receiver sensitivity constraint; and (ii) the extra losses experienced by the express signal when traversing the splitter and the combiner mitigate the power level at the input of the next fiber, which assists in the task of operating with negligible impact from nonlinear interference. In the rest of the paper, we only consider the pre-amplifier configuration.

Fig. 3(a) shows the average minimum number of amplifiers deployed in horseshoe networks with 5, 10, and 15 leaf nodes when different sets of candidate splitter/combiner types are considered. Also, 95% confidence intervals are shown as error bars. In general, it can be observed that the number of optical amplifiers increases when the number of leaf nodes increases or the diversity of available splitter/combiner ratios decreases. When all the splitters/combiners listed in Table 1 are considered in the optimization (referred to as scenario1), the average number of amplifiers increases from about 2 to 5.2 when the number of leaf nodes increases from 5 to 15. In general, using certain ratios of splitters/combiners reduces the number of amplifiers by more than 50%. The small increase in the number of amplifiers in Scenario2 over Scenario1 suggests that the support of only two (carefully selected) splitting ratios allows the realization of most of the amplifier savings while avoiding the complexity of deploying and maintaining spares for many device types. Interestingly, although both Scenario3 and Scenario4 only allow the deployment of one splitter/combiner, Scenario3 is more flexible than Scenario4 because the port allocation of 90/10 splitters/combiners allows either minimizing the losses in the add/drop path or minimizing the losses in the express path. As a result, in Scenario3 the number of amplifiers is 10%-30% less than that in Scenario4.

Fig. 3(b) illustrates the average maximum power difference between SCs at the input of Hub2 Rx for all scenarios and considered network sizes. All the values fall below 8 dB as per constraint (16) imposed by the ILP model. However, as explained above, further reducing this difference can help the receiver to operate closer to optimal conditions and this motivates including it as a secondary objective function in the ILP model. It can be seen that as the network size increases, the maximum power difference between SCs tends to increase, an expected consequence of having SCs that have to traverse significantly longer upstream paths and traverse more splitters/combiners. Importantly, when considering Scenarios 1, 2 and 3, it can be seen that the higher diversity of available splitter/combiner types usually

Table 2. Number of amplifiers and maximum SCs power difference with pre-amplifier and booster-amplifier configurations for two scenarios.

	Pre-amplifier		Booster-amplifier	
	# of amplifiers	Maximum SCs power difference	# of amplifiers	Maximum SCs power difference
Scenario1: All	3.9	2.2	5.5	3
Scenario2: 70/30 & 90/10	4.1	2.9	7	3.9

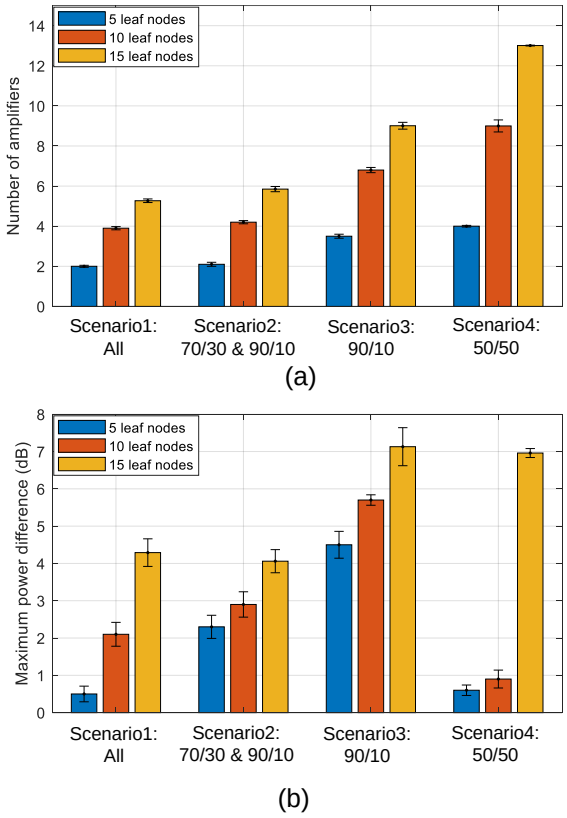

Fig. 3. (a) Minimum number of amplifiers and (b) maximum power difference of SCs at Hub2 Rx versus set of candidate splitter/combiner types used in horseshoe network.

enables a reduction in the maximum power difference between SCs. However, since minimizing amplifier count always takes precedence over minimizing the maximum power difference between SCs, in some cases the expected behavior – smaller networks and higher diversity of splitter/combiner types leading to lower figures of the latter metric – may not hold. This is particularly evident for Scenario4, which only supports one splitter/combiner type but allows the attaining of the lowest value for the maximum power difference between SCs among all scenarios, when considering networks with 5 and 10 leaf nodes. By examining these cases, it is observed that in general, only one amplifier is saved in both cases, namely the one located at the first leaf node. Since this amplifier does not provide gain to any upstream SCs, it is not useful for minimizing SC power unbalance. Moreover, the fact that amplifiers are placed in all the other leaf nodes maximizes the degrees of freedom to reduce the power imbalance via the amplifiers' gain values. In networks with 15 leaf nodes and enforcing Scenario4, the total number of amplifiers is around 13, so at least one additional amplifier, besides the one at the first leaf node, is saved. This reduction has an immediate impact on the ability to minimize the maximum power difference between SCs as well, given that, in this scenario, it is not possible to leverage different splitter/combiner types and their port allocation to further adjust losses in the add and express paths.

Figure 4 depicts the loss of links, add/drop loss (excess loss included), and leaf nodes' losses for transit signals in a 10-leaf node network, optimized for both Scenario1 and Scenario4. In Scenario1, although the number of amplifiers is lower, their gain values are higher compared to Scenario4. Power calculation is shown for SCs launched by Hub1 to leaf2 and from leaf8 to Hub2. Additionally, most of the leaf nodes employ splitters/combiners with lower ratios for add/drop functions, resulting in reduced leaf loss across the optical link. These findings emphasize the significance of the range of amplifiers' gain. For example, if the maximum amplifiers' gain is limited to 14 dB, then five amplifiers would be required in Scenario1 instead of four.

Fig. 5 shows the average total OSNR of downstream SCs at the leaf nodes' receivers in different splitter/combiner scenarios, when considering 10-leaf node horseshoe topologies. Downstream SCs, i.e., SCs going from Hub1 to leaf nodes, are amplified together and also dropped together at the leaf nodes. As expected, the total OSNR decreases when a leaf node's distance to Hub1 increases. The minimum average OSNR is observed for leaf 10 in the 50/50 scenario, and it is about 18 dB, which is still higher than the 12 dB OSNR tolerance. The total value of the OSNR depends on the number of amplifiers traversed and their individual OSNR contribution (Eq. 19). The individual OSNR values depend on the power of a particular SC at the amplifiers' input as shown in Eq. 18 (link length and selection of splitters/combiners affect the amount of loss and consequently the input's power). Scenario4 leads to the lowest average total OSNR since the number of amplifiers is around 9 (see Fig. 3). Scenario3 results in the highest average total OSNR for all leaf nodes despite requiring more amplifiers than in Scenario1 and Scenario2. To justify this, 10% ports of combiners and splitters are often employed as add and drop, while ports with a 90% ratio are deployed as express. As a result, the in-line loss is lower, which leads to higher amplifiers' input power and higher individual OSNRs.

When an EDFA is placed in the horseshoe, a broadband unfiltered ASE noise is also introduced. Since we are considering a filterless transmission network scenario, this ASE noise is never blocked and always reaches the hub node in the upstream direction (from leaf nodes to hub). Consequently, at the receiver located in Hub2, the ASE noise level remains constant across the complete transmission bandwidth. Therefore, the OSNR variation between the different SCs is equal to the power difference between SCs only, independently of their point of origin (leaf node). Through extensive simulation, we found that the OSNR

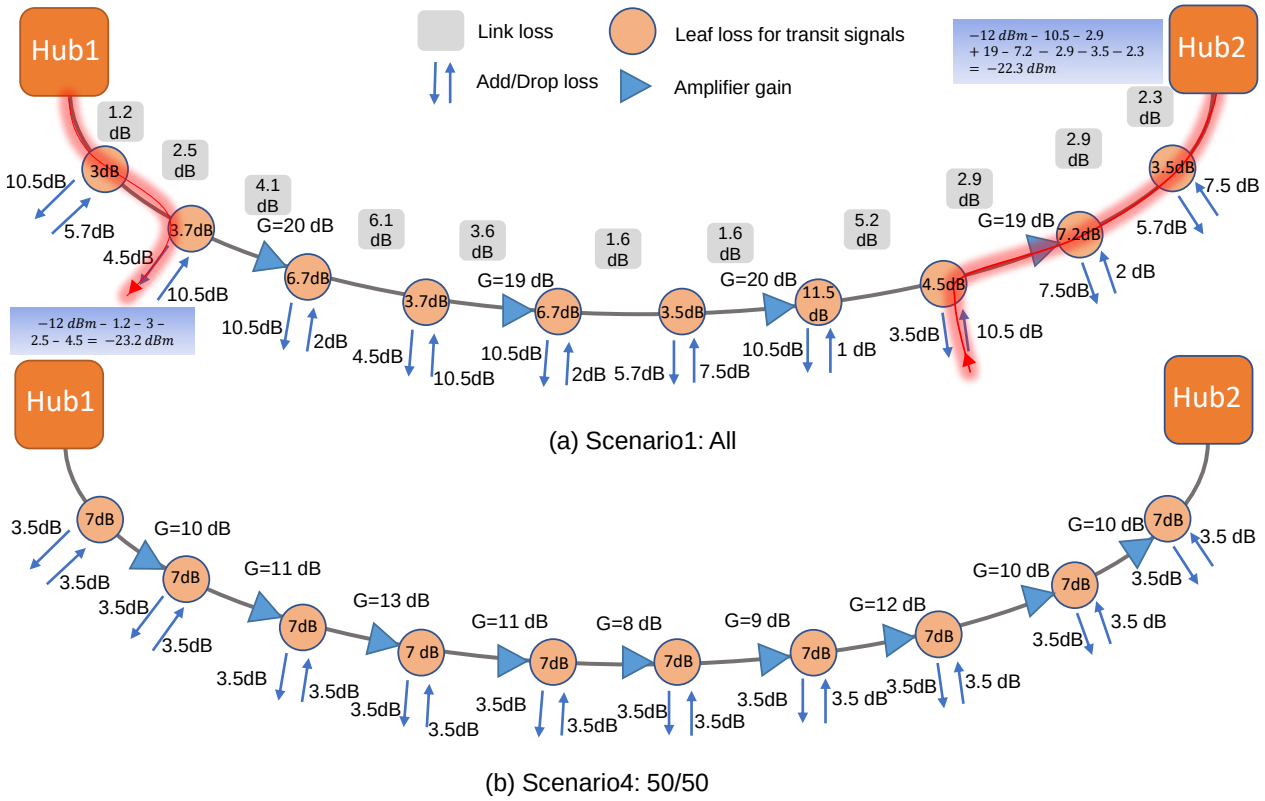

Fig. 4. Characterization of losses and gains for an optimized instance of 10-leaf node network (optical fiber link directed from Hub1 to Hub2) for (a) Scenario1 and (b) Scenario4.

always exceeded 20 dB across all transmission scenarios and network instances for the SC originating in the first leaf node. Since the SCs power difference must be smaller than 8 dB, as imposed by the ILP model, it can be asserted that the OSNR for all other leaf nodes is always greater than 12 dB threshold. It is noteworthy that, for both downstream and upstream transmission, the analysis shows that the required OSNR of a DSCM-based P2MP transceiver (assumed to have similar performance to that specified by 400G OpenZR+ MSA [33]) can be met. However, this might not always be the case and if OSNR values fall below the threshold, the design would not have been valid and alternative ways would have to be employed. Two main options can be envisioned to address this possible issue. One would be iteratively running the ILP model, validating the OSNR and if for some leaf nodes the OSNR threshold is not met, enforcing certain decisions and running again the model with additional constraints. The other main option, now being pursued, is to rely on a meta-heuristic method (e.g., a genetic algorithm) [36, 37], instead of an ILP, and embedding the OSNR validation in the process of assessing the quality (e.g., fitness) of each solution being generated.

To gain further insight into the usage of the different splitter/combiner types, Table 3 presents the utilization ratios of various splitter and combiner configurations in both Scenario1 and Scenario2 for horseshoe topologies comprising 10 leaf nodes. The results indicate that 80/20 splitters and combiners are the most utilized in Scenario1, with minimal utilization of 50/50 splitters and combiners. Conversely, Scenario2 displays a higher usage of 70/30 splitters and combiners. These results suggest that the most utilized type of splitter/combiner tends to be the

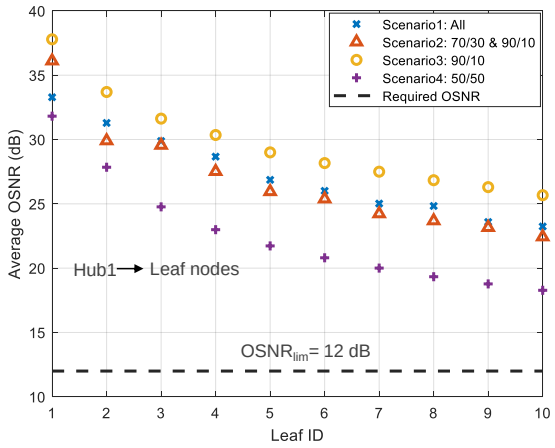

Fig. 5. Average OSNR of optical SCs transmitted from Hub1 to leaf nodes in 10-leaf node horseshoe networks.

one that offers some degree of imbalance in power losses per port (but not necessarily the highest degree).

Table 4 shows the average solving time and the standard deviation of 100 runs of the ILP model when considering Scenario1, which has more variables than the other scenarios, and networks with different numbers of leaf nodes using a typical laptop with 16GB RAM and a Core i7 @1.8 GHz CPU. As can be seen, the solving time rapidly increases with the increase of the network size

Table 3. Usage percentage of the different splitter/combiner types in 10-leaf horseshoe networks obtained by 100 simulations when all splitters/combiners considered as well as only 70/30 and 90/10.

		90/10	80/20	70/30	60/40	50/50
Scenario1	Combiners	30%	36%	21%	10%	3%
	Splitters	29%	32%	21%	12%	6%
Scenario2	Combiners	43%		57%		
	Splitters	42%		58%		

and consequently the number of variables and constraints. In networks with 15 leaf nodes, there are some problem instances that take a longer time to solve, reflected in the significantly higher standard deviation value. Note that ILP is classified as an NP-hard problem [38], which means that finding an optimal solution can be extremely difficult and time-consuming for large-scale problems. In addition, non-linear constraints can be modeled with ILP methods and, as previously mentioned, other approaches, such as heuristics, would have to be employed.

Table 4. Average and standard deviation of the ILP model solving time for the Scenario1 and networks with 5, 10, and 15 leaf nodes.

Network Size (# of leaf nodes)	5	10	15
Number of Variables	215	430	645
Number of Constraints	81	186	316
Average Solving Time (second)	4.03	9.32	52.44
Std of Solving Time (second)	0.92	1.23	105.23

6. CONCLUSIONS

This paper focused on designing and optimizing a filterless architecture for metro-aggregation networks featuring a horseshoe topology and supporting DSCM-based P2MP transceivers. To optimize the design for different network sizes and scenarios with different sets of available splitter/combiner types, an integer linear programming (ILP) framework is described. The primary objective of the ILP model is to minimize the number of optical amplifiers required, while also minimizing the maximum power difference at the hub's receiver input. The framework includes several constraints to ensure the feasibility of the resulting line system configuration. The results of the optimization, obtained over a large number of problem instances, demonstrate that it is possible to leverage the splitter/combiner type diversity to realize savings in the number of optical amplifiers. Moreover, the results also show that it is possible to have configurations that feature a trade-off between realizing most of the amplifier savings while relying only on a few different splitter/combiner types. In future work, we plan to investigate incorporating OSNR approximations into the ILP model and exploring heuristic solutions such as genetic algorithm to address more complex network deployments.

FUNDING

This work received funding from EU Horizon 2020 program under the MSCA grant agreement No. 813144 (REAL-NET). SKT acknowledges the support of the EPSRC project TRANSNET. J. Pedro, A. Napoli and N. Costa would like to thank the European Commission for funding their activities through the H2020 B5G-OPEN (G.A. 101016663). J. Pedro also acknowledges the partial support of Fundação para a Ciência e Tecnologia (FCT) project UIDB/50008/2020.

REFERENCES

1. T. Horvath, P. Munster, V. Oujezsky, and N.-H. Bao, "Passive optical networks progress: a tutorial," Electronics **9**, 1081 (2020).
2. J. Bäck, A. Napoli, E. Riccardi, M. Quagliotti, M. Porrega, J. Pedro, T. A. Eriksson, F. Masoud, A. Mathur, and D. Welch, "A filterless design with point-to-multipoint transceivers for cost-effective and challenging metro/regional aggregation topologies," in 2022 International Conference on Optical Network Design and Modeling (ONDM), (IEEE, 2022), pp. 1–6.
3. P. Pavon-Marino, N. Skorin-Kapov, M. Bueno-Delgado, J. Bäck, and A. Napoli, "On the benefits of point-to-multipoint coherent optics for multilayer capacity planning in ring networks with varying traffic profiles," J. Opt. Commun. Netw. **14**, B30–B44 (2022).
4. M. M. Hosseini, J. Pedro, N. Costa, A. Napoli, J. E. Prilepsky, and S. K. Turitsyn, "Optimized physical design of metro aggregation networks using point to multipoint transceivers," in Optical Fiber Communication Conference, (Optica Publishing Group, 2022), pp. W3F–2.
5. H. S. Abbas and M. A. Gregory, "The next generation of passive optical networks: A review," J. network computer applications **67**, 53–74 (2016).
6. D. F. Welch, "Disruption cycles for optical networks: How point to multi-point coherent optics can transform the cost and complexity of the optical network," in 2020 European Conference on Optical Communications (ECOC), (IEEE, 2020), pp. 1–3.
7. D. Welch, A. Napoli, J. Bäck, S. Buggaveeti, C. Castro, A. Chase, X. Chen, V. Dominic, T. Duthel, T. A. Eriksson et al., "Digital subcarrier multiplexing: Enabling software-configurable optical networks," J. Light. Technol. **41**, 1175–1191 (2023).
8. M. M. Hosseini, J. Pedro, A. Napoli, N. Costa, J. E. Prilepsky, and S. K. Turitsyn, "Design of survivable metro-aggregation networks based on digital subcarrier routing," in 2021 IEEE Global Communications Conference (GLOBECOM), (IEEE, 2021), pp. 1–6.
9. M. M. Hosseini, J. Pedro, A. Napoli, N. Costa, J. E. Prilepsky, and S. K. Turitsyn, "Optimization of survivable filterless optical networks exploiting digital subcarrier multiplexing," J. Opt. Commun. Netw. **14**, 586–594 (2022).
10. X. Sun, C.-K. Chan, and L. K. Chen, "A survivable WDM-PON architecture with centralized alternate-path protection switching for traffic restoration," IEEE Photonics Technol. Lett. **18**, 631–633 (2006).
11. E. Wong, E. Grigoreva, L. Wosinska, and C. M. Machuca, "Enhancing the survivability and power savings of 5g transport networks based on DWDM rings," J. Opt. Commun. Netw. **9**, D74–D85 (2017).
12. G. Shen, H. Guo, and S. K. Bose, "Survivable elastic optical networks: survey and perspective," Photonic Netw. Commun. **31**, 71–87 (2016).
13. M. M. Hosseini, J. Pedro, N. Costa, A. Napoli, J. E. Prilepsky, and S. K. Turitsyn, "Optimal design of filterless horseshoe networks supporting point-to-multipoint transceivers," in 2023 Optical Fiber

Communications Conference and Exhibition (OFC), (IEEE, 2023), pp. 1–3.
14. A. V. Tran, R. S. Tucker, and N. L. Boland, "Amplifier placement methods for metropolitan WDM ring networks," J. Light. Technol. **22**, 2509 (2004).
15. M. Ibrahimi, O. Ayoub, F. Musumeci, O. Karandin, A. Castoldi, R. Pastorelli, and M. Tornatore, "Minimum-cost optical amplifier placement in metro networks," J. Light. Technol. **38**, 3221–3228 (2020).
16. A. Dochhan, R. Emmerich, P. W. Berenguer, C. Schubert, J. K. Fischer, M. H. Eiselt, and J.-P. Elbers, "Flexible metro network architecture based on wavelength blockers and coherent transmission," in 45th European Conference on Optical Communication (ECOC 2019), (IET, 2019), pp. 1–4.
17. F. Paolucci, R. Emmerich, A. Eira, N. Costa, J. Pedro, P. W. Berenguer, C. Schubert, J. Fischer, F. Fresi, A. Sgambelluri et al., "Disaggregated edge-enabled C+L-band filterless metro networks," J. Opt. Commun. Netw. **12**, 2–12 (2020).
18. A. Nespola, L. Bertignono, G. Bosco, A. Carena, Y. Jiang, S. M. Bilal, P. Poggiolini, S. Abrate, and F. Forghieri, "Experimental demonstration of fiber nonlinearity mitigation in a WDM multi-subcarrier coherent optical system," in 2015 European Conference on Optical Communication (ECOC), (IEEE, 2015), pp. 1–3.
19. M. Qiu, Q. Zhuge, X. Xu, M. Chagnon, M. Morsy-Osman, and D. V. Plant, "Subcarrier multiplexing using dacs for fiber nonlinearity mitigation in coherent optical communication systems," in Optical Fiber Communication Conference, (Optica Publishing Group, 2014), pp. Tu3J–2.
20. W. Shieh and Y. Tang, "Ultrahigh-speed signal transmission over nonlinear and dispersive fiber optic channel: The multicarrier advantage," IEEE Photonics J. **2**, 276–283 (2010).
21. M. Qiu, Q. Zhuge, M. Chagnon, Y. Gao, X. Xu, M. Morsy-Osman, and D. V. Plant, "Digital subcarrier multiplexing for fiber nonlinearity mitigation in coherent optical communication systems," Opt. Express **22**, 18770–18777 (2014).
22. H. Sun, M. Torbatian, M. Karimi, R. Maher, S. Thomson, M. Tehrani, Y. Gao, A. Kumpera, G. Soliman, A. Kakkar et al., "800g dsp asic design using probabilistic shaping and digital sub-carrier multiplexing," J. Light. Tehnology **38**, 4744–4756 (2020).
23. D. Krause, A. Awadalla, A. S. Karar, H. Sun, and K.-T. Wu, "Design considerations for a digital subcarrier coherent optical modem," in 2017 Optical Fiber Communications Conference and Exhibition (OFC), (IEEE, 2017), pp. 1–3.
24. J. Pedro, "Comparative assessment of 800G-capable embedded and pluggable coherent line interfaces over the optical network lifecycle," in Asia Communications and Photonics Conference, (Optica Publishing Group, 2022), p. 9361.
25. I. Cale, A. Salihovic, and M. Ivekovic, "Gigabit passive optical network-GPON," in 2007 29th International Conference on Information Technology Interfaces, (IEEE, 2007), pp. 679–684.
26. A. Agata and Y. Horiuchi, "PON network designing algorithm for suboptimal deployment of optical fiber cables," in 2009 Asia Communications and Photonics conference and Exhibition (ACP), vol. 2009 (IEEE, 2009), pp. 1–6.
27. A. Kawakita, K. Hara, Y. Kimura, K. Horikawa, H. Furukawa, Y. Suzuki, and S. Ikeda, "Design for long-reach coexisting PON in consideration of area characteristics with wavelength selective asymmetrical splitters," in 2019 24th OptoElectronics and Communications Conference (OECC) and 2019 International Conference on Photonics in Switching and Computing (PSC), (IEEE, 2019), pp. 1–3.
28. K. Grobe and J.-P. Elbers, "PON in adolescence: from TDMA to WDM-PON," IEEE Commun. Mag. **46**, 26–34 (2008).
29. É. Archambault, D. O'Brien, C. Tremblay, F. Gagnon, M. P. Bélanger, and É. Bernier, "Design and simulation of filterless optical networks: Problem definition and performance evaluation," J. Opt. Commun. Netw. **2**, 496–501 (2010).
30. Y. Park, C. Lim, and I. Jung, "ONU power equalization of ethernet PON systems," IEEE Photonics Technol. Lett. **16**, 1984–1986 (2004).
31. M. Dalla Santa, C. Antony, G. Talli, and P. D. Townsend, "Variable gain SOA pre-amplifier for optical equalization of a 25gb/s burst-mode PON upstream with 10g optics," in 2019 Optical Fiber Communications Conference and Exhibition (OFC), (IEEE, 2019), pp. 1–3.
32. S. K. Routray, R. M. Morais, J. R. F. da Rocha, and A. N. Pinto, "Statistical model for link lengths in optical transport networks," J. Opt. Commun. Netw. **5**, 762–773 (2013).
33. "Openzr+ 400g digital coherent optics for multi-haul," https://openzrplus.org/site/assets/files/1074/openzrplus_whitepaper_-_sept_29_2020_final.pdf.
34. J. A. Besley, J. D. Love, and W. Langer, "A multimode planar power splitter," J. Light. Technol. **16**, 678–684 (1998).
35. J. Teng, J. Yang, C. Lv, T. Chen, J. Guo, J. Feng, and P. Wu, "Guidelines for design and fabrication of fused fiber coupler based wavelength division multiplexings," Opt. Fiber Technol. **20**, 239–244 (2014).
36. M. Ibrahimi, O. Ayoub, O. Karandin, F. Musumeci, A. Castoldi, R. Pastorelli, and M. Tornatore, "Qot-aware optical amplifier placement in filterless metro networks," IEEE Commun. Lett. **25**, 931–935 (2020).
37. E. K. H. Ng and C. G. Kelly, "Method for determining location and gain settings of amplifiers in an optical network by using a genetic algorithm," (2006). US Patent 7,038,837.
38. A. Paulus, M. Rolínek, V. Musil, B. Amos, and G. Martius, "Comboptnet: Fit the right np-hard problem by learning integer programming constraints," in International Conference on Machine Learning, (PMLR, 2021), pp. 8443–8453.